P4.10

STUDY OF THE PDFs OF A STABLY STRATIFIED LARGE-EDDY SIMULATION

M.A. Jiménez * and J. Cuxart

Universitat de les Illes Balears, Spain

1 INTRODUCTION

Several studies of turbulent flows using Probability Density Functions (PDFs) have been made with observational data, such as in Mahrt and Paumier (1984), and with physical laboratory experiments. Here an attempt to compute PDFs from a high resolution Large-Eddy Simulation (LES) of a stably stratified boundary layer (SBL) is made.

The GABLS (GEWEX Atmospheric Boundary Layer Studies, of the World Meteorological Organization) action intends to improve the understanding of the Atmospheric Boundary Layer (ABL) and its representation in regional and large scale climate models. It has proposed a simplified non-strongly stably stratified regime to check the performance of the LES models (Beare et al, 2004). The PDFs for this case will be computed and compared to those for a LES of a zero-mean wind Convective Boundary Layer case (ZW-CBL, Nieuwstadt et al, 1993). In this case, the PDFs of the temperature and the vertical wind and their joint PDF give qualitatively similar results to those found by Deardorff and Willis (1985, DW85 from now on) for a tank experiment, and to those of Chu et al. (1996) for field measurements near the ground.

The eddy structures of the SBL case will be studied through the PDFs and some further statistics will be computed and compared to ZW-CBL. The PDFs depend on the simulated eddy structures within the LES, that are strongly conditioned by the subgrid scheme, and this fact must be kept in mind during the analysis. Furthermore, the effect of a change of the LES resolution on the PDFs will be explored, as well as the issue of the ergodicity, by comparing ensemble averages to space and time averages.

*Corresponding author address: Maria Antónia Jiménez, Grup de Meteorologia, Dpt. Fisica, Universitat de les Illes Balears, Carret. Valldemossa, km 7.5, 07122-Palma de Mallorca, Spain; email:mantonia.jimenez@uib.es

2 LARGE EDDY STRUCTURES AND PDFS

The runs have been done with the MESO-NH model (Lafore et al., 1998; Cuxart et al, 2000). The results of the GABLS SBL case at a resolution of 3.125 m are used, whereas the ZW-CBL has been performed at a resolution of 50 m. Three levels have been selected, one near the surface (z/zi=0.1), another in the interior of the ABL (z/zi=0.5) and another one at the upper part of the inversion (z/zi = 1.1) where zi is the value of the boundary layer height. The corresponding horizontal cross-sections for the u component of the wind are displayed in Figure 1 for the SBL run.

For the SBL, the PDFs are computed for the three components of the wind (u, v, w) and θ at the 3 levels considered, taking one field every minute during the eighth hour of integration. Therefore $128\times128\times60$ different points are used to construct each PDF. The same is done for the fourth hour of the ZW-CBL run that uses an equivalent domain (128×128 points for each horizontal slice) and at the same temporal frequency (one field every minute). In Figure 2 the resulting PDFs for u (B(u)) of the SBL are given.

Within the SBL, the structures are caracterized by the appearance of alternating streaks of high and low speed aligned in the mean flow direction near the surface; a level where the eddies are smaller than in the middle of the SBL. The upper horizontal cross-section shows that this level has turbulent structures that emerge from the SBL into the layer above the ondulating inversion and areas without turbulence.

In the u-component horizontal cross-section near the ground (Figure 1.a) the values are more spread out than in higher levels where the wind does not change much along the field (Figure 1.c). Therefore, near the ground σ is larger (Table I) than in the top of the boundary layer where the values are more concentrated close to the mean.

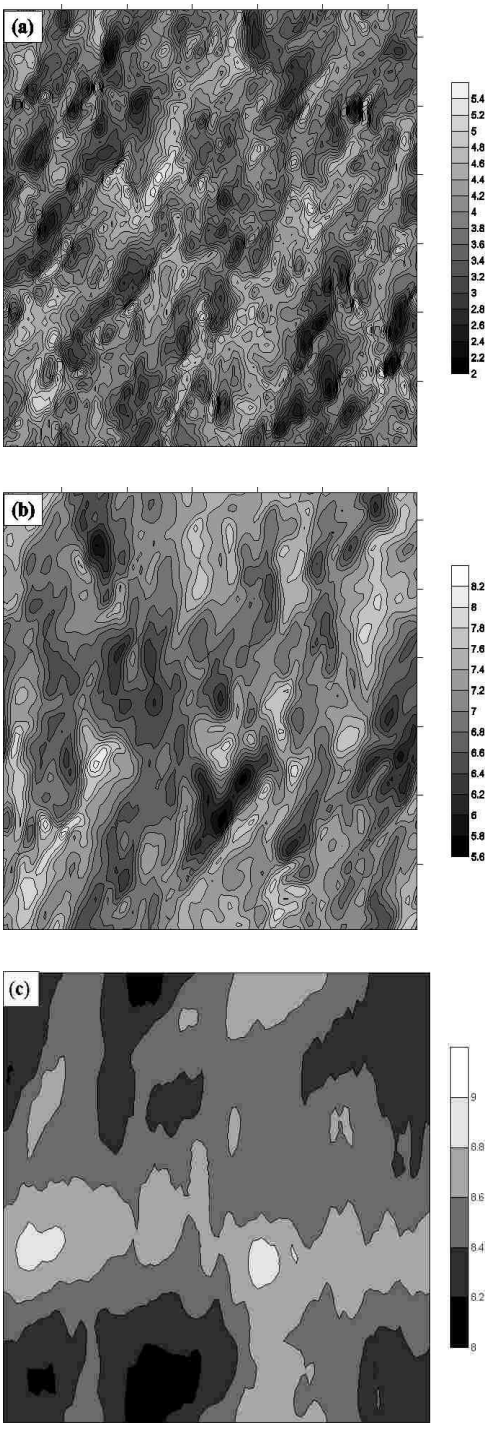

Figure 1: u-component of the wind horizontal cross-sections for the GABLS at the studied levels (one line each 0.2 m s^{-1}).

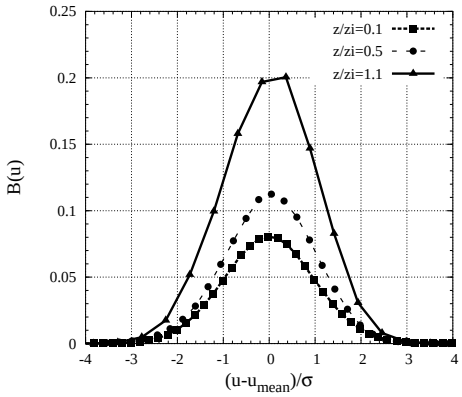

Figure 2: PDFs for u obtained from the 3.125 m resolution GABLS case for the three levels considered, normalized by the respective mean value and σ.

The probability of the most frequent values increases with height (Figure 2) which is consistent with a corresponding decrease of the spread.

On the other hand, the turbulent structures in the stable case are smaller sized than those computed for ZW-CBL and those observed in the tank (DW85) and by Chu et al (1996) for weak wind unstable conditions. Besides, the SBL structures have updrafts and downdrafts of a similar area and intensity, contrarily to the large assymetry found in the ZW-CBL between the strong narrow updrafts and the wide slow downdrafts,

3 STATISTICS OBTAINED FROM THE PDFS

The statistical momenta computed from the PDFs of the SBL are shown in Table 1 (up to the fourth order) for u at the three levels of interest.

Table 1: $\overline{u}$ wind component statistics of the stable GABLS case computed through PDF. In brackets ($\bar{u}_{PDF}$-$\bar{u}_{LES}$).

	z/zi=0.1	z/zi=0.5	z/zi=1.1
$\bar{u}$ (m s^{-1})	3.859(0.008)	7.032(-0.013)	8.480(0.000)
σ (m s^{-1})	0.501(-0.022)	0.362(-0.010)	0.191(0.016)
S	0.037	-0.168	-0.099
K	3.081	3.195	2.846

A normal distribution has zero skewness (S) and a kurtosis (K) value of 3. The large number of small structures near the ground have a near-normal distribution as S and K indicates and also

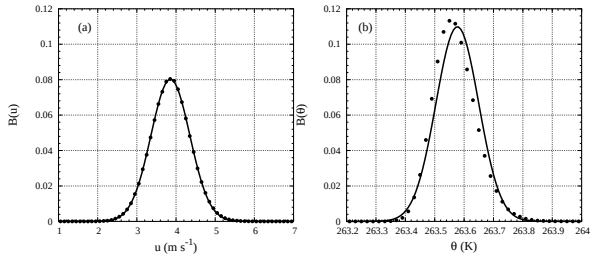

Figure 3: Gaussian fit of (a) u and (b) θ PDFs for the GABLS case near the ground.

high values for σ (the square-root of the variance) The differences of the mean and σ values in respect to those computed classically in the LES are relatively small.

In the middle of the SBL there are less u structures and each structure occupies a larger area than those near the ground. Therefore, σ is smaller and the departure from the normality is large, specially concerning the assymetry, since the skewnees is negative and large, indicating that there is predominancy of values smaller than the average.

In the upper part of the top temperature inversion, there are less structures and the fact that the PDF is narrow means that the turbulence is located in specific areas surrounded by areas of almost constant values, as it is also seen in the cross-section in Figure 1.

The picture suggests eddies of u more active near the ground, with just some of them reaching larger heights and progressively less distinguishable of the mean flow. The warmer air comes from above and is mixed downwards by the large eddies until it reaches the surface layer, where it is very effectively diffused by the small scale structures, together with the cold air coming from the surface. This is a very different picture from the CBL case, with narrow and strong updrafts and slow and wide downdrafts, leading to significantly larger values for σ and the skewness.

3.1 Gaussianity of the PDFs and characteristic functions

It has been shown above that the PDFs are approximately normal, since their shapes, skewness and kurtosis do not depart much from those corresponding to a gaussian. The Kolmogorov-Smirnov test (Wilks, 1995) is used to check their gaussianity. All the PDFs are considered gaussian by this test if a rejection level of 5% is taken, except the temperature near the ground, where the skewness is very large.

Table 2: σ for wind components (in m s^{-1}) and temperature (in K) computed through the characteristic function at z/zi=0.1, 0.5, 1.1 for 3.125 m resolution GABLS case. In brackets (σ_{PDF}-σ_{LES}).

	z/zi=0.1	z/zi=0.5	z/zi=1.1
σ_θ	0.052(-0.020)	0.060(-0.027)	0.086(-0.034)
σ_u	0.350(-0.151)	0.250(-0.112)	0.138(-0.053)
σ_v	0.291(-0.123)	0.176(-0.077)	0.062(-0.026)
σ_w	0.182(-0.084)	0.123(-0.061)	0.074(-0.032)

The fit of the PDF to a gaussian shape is shown in Figure 3 for u and θ near the ground. It is clear that $\theta(0.1z_i)$ does not fit well to the gaussian because of its negative and large skewness, very similarly to what happens for ZW-CBL.

The Fourier transform of the PDF is called the characteristic function ($\phi(k)$), where $k = \frac{2\pi}{U_{max}-U_{min}} n\Delta u$ is the wavenumber, $n = 1, ..., \frac{U_{max}-U_{min}}{\Delta u}$ and $\Delta u = 0.1$ m s^{-1}. Here $\phi(k)$ is computed taking the gaussian fits of the PDFs and obtaining their analytical Fourier transforms and then the turbulence momenta are computed from the derivates (Tennekes and Lumley, 1972).

Table 2 shows the standard deviations computed by this method. The differences with the values computed directly from the PDF are of about one third to one half and the standard deviations are systematically underestimated. We can conclude that, although the PDFs fit approximatively well to a normal distribution, to treat them as gaussian curves leads to the underestimation of the values of the turbulence momenta if obtained through the characteristic function.

4 JOINT PDFS

In this section we will focus on the Joint PDFs of w and θ (B(u,θ), Figure 4) to inspect how well correlated are w and θ. The vertical temperature flux is the first joint moment (covariance or correlation) computed from $B(w, \theta)$.

Following Mahrt and Paumier (1984, MP84) the geometry of the joint PDF is explored. Completely random motions (phase lags of 90 °) would yield joint PDF formed by a variety of circles so that the density function depends only on the distance from the origin. Periodic motions with phases other than 0, 90, 180 and 270 ° correspond

Table 3: Vertical temperature flux (in K m s^{-1}) obtained from the Joint PDFs. In brackets ($\overline{w\theta}_{PDFs}$ - $\overline{w\theta}_{LES}$)

	$\overline{w\theta}$
z/zi=0.1	-0.0086(-0.0010)
z/zi=0.5	-0.0050(-0.0001)
z/zi=1.1	-0.0003(0.0001)

to partial correlation and elliptical patterns of the joint PDF, which is the expected case for the turbulent stratified flows. The most vigorous events are associated with the largest distances to the origin. Figure 4 can be compared to Figure 3 of MP84 and interpreted in terms of quadrants. The upper right quadrant ($w' > 0$, $\theta' > 0$) corresponds to warm updrafts, the upper left one ($w' > 0$, $\theta' < 0$) to cold updrafts and so on. For a given distance from the origin, the flux is greatest for an angle of 45, 135, 225 or 315 °, since these are the axes of maximum correlation. For a given angle, the generation of flux increases with the radial distance.

Near the ground the joint PDF is tilted about 10 ° towards the bottom left quadrant, correponding to the predominancy of warm downdrafts and cold updrafts, in good agreement with the picture outlined above. In the middle of the SBL, the tilt varies to 6 ° still to the same quadrants but with smaller distances to the origin. In the inversion layer, there is almost no tilt corresponding to a very small correlation between w and θ. If the actual values of the fluxes are computed, they are very similar to those given by the standard LES method, slightly weaker near the ground, practically equal in the middle of the SBL and a 33% stronger at the inversion layer.

For the ZW-CBL case, the PDFs are similar to those obtained by DW85 in the middle and the inversion layer and by Chu et al (1996) near the ground. Despite the fact that the correlation between w and θ decreases with height as in the GABLS case, within the boundary layer the correlation is positive whereas in the top of the boundary layer is negative due to the negative flux in the entrainment zone.

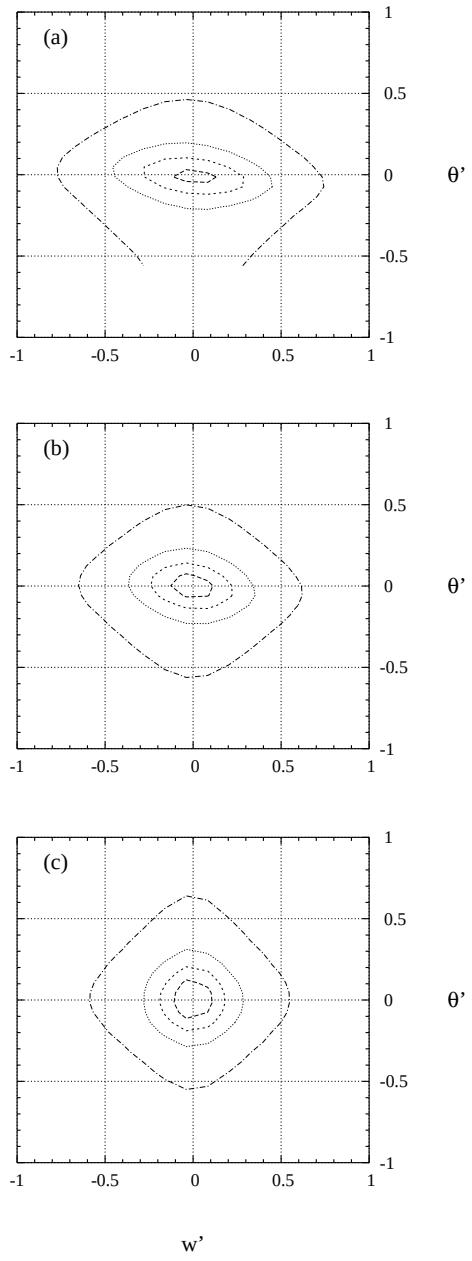

Figure 4: Joint PDFs of w and θ obtained from GABLS at (a) z/zi=0.1,(b) z/zi=0.5 and (c) z/zi=1.1. The contours start at 0.0001 level with incrementals of 0.0001 until 0.0004 in each case. The variables are normalized by the respective mean values and σ: $w' = (w - \bar{w})/\sigma_w$ and $\theta' = (\theta - \bar{\theta})/\sigma_\theta$.

5 ERGODICITY

The applicability of the ergodic theorem for the LESs under study will be now checked. The following quantities are considered for the three levels of analysis: i) the approximate "ensemble average" operator, $\mathcal{M}(x,t)$, built using the complete fields at each level and using one output every minute for a whole hour. ii) the approximate "spatial average" operator, $\mathcal{M}(x)$, that takes a field at each level for one single instant; iii) the approximate "temporal average" operator, $\mathcal{M}(t)$, that takes all the values during one hour for one specific point.

$\mathcal{M}(x,t)$=$\mathcal{M}(t)$ means that the variable is homogeneous whereas $\mathcal{M}(x,t)$=$\mathcal{M}(x)$ implies stationarity. Ergodicity occurs when stationarity and homegeneity take place simultaneously.

The PDFs for u of the three different operators for the SBL are shown in Figure 5, corresponding to the ensemble average, the spatial operator applied at three different instants of the eighth hour (15', 30' and 45') and the temporal operator at two different points of the domain. The averages are written in Table 4.

Table 4: $\overline{u}$ (in m s^{-1}) computed from $\mathcal{M}(x,t)$, $\mathcal{M}(x)$ and $\mathcal{M}(t)$.

	z/zi=0.1	z/zi=0.5	z/zi=1.1
$\mathcal{M}(x,t)$	3.86	7.03	8.48
$\mathcal{M}(t1)$	3.87	7.02	8.48
$\mathcal{M}(t2)$	4.34	7.37	8.08
$\mathcal{M}(x15)$	3.80	7.06	8.45
$\mathcal{M}(x30)$	3.89	7.02	8.49
$\mathcal{M}(x45)$	3.85	7.08	8.49

As shown in Beare et al (2004), the regime is stationary from the 7th hour on. This is confirmed here by the fact that the PDFs for the different instants ($\mathcal{M}(x15, x30, x45)$) are very similar to the one for the ensemble of the hour ($\mathcal{M}(x,t)$). However the PDFs and the mean values obtained for the temporal series ($\mathcal{M}(t1, t2)$) diverge significantly. It is concluded that the field is not homogeneous and therefore the ergodic theorem is not fulfilled for such a regime. As the pair of updrafts-downdrafts are more intense in the CBL, the field is less homogeneous than for the SBL and it is even further away from the ergodicity.

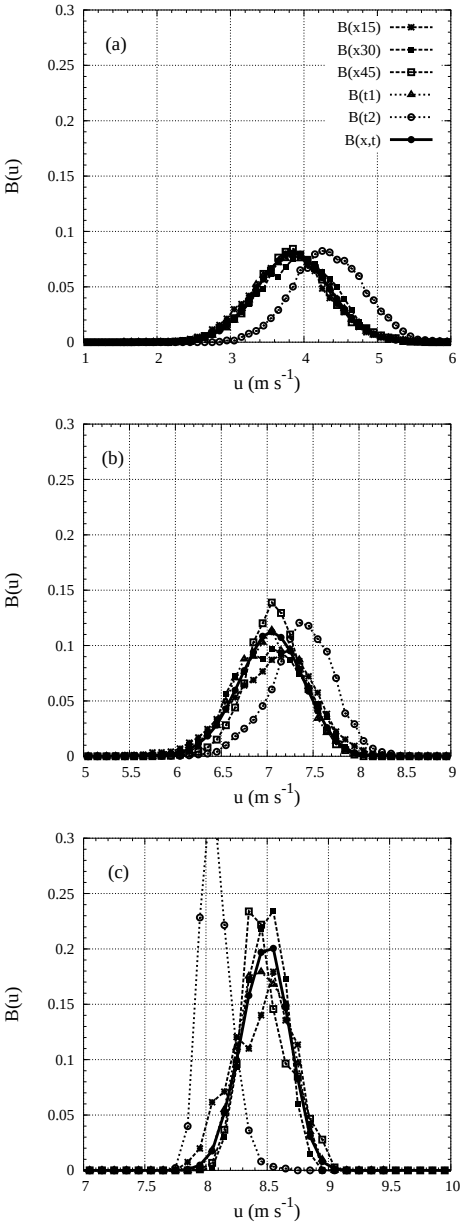

Figure 5: Ergodic theorem for u at the three studied levels. In circles $\mathcal{M}(x,t)$, in squares $\mathcal{M}(x)$ and in triangles $\mathcal{M}(t)$

6 SENSITIVITY TO RESOLUTION

As the resolution decreases without changing the domain size the PDFs are built with a much smaller number of points. In our case using 32×32 points in a horizontal slice implies a PDF computed with 1024 points instead of the 16384 points for the 128×128 case for a single instant. Besides, the smallest scales are not represented in the degraded resolution case and this can alter the distribution of the larger structures. When the PDFs are compared, the degraded resolution run has skewness and kurtosis values larger, mostly near the surface, where the shape of the PDF becomes flatter. The worse defined structures reduce the heterogeneity of the fields and the departure from ergodicity is smaller; in this sense approaching the ergodicity is not synonim of a more realistic simulation.

7 CONCLUSIONS

The study of the SBL GABLS case through PDFs complements the information provided by the classical LES averages and allows to summarize the information about the observed eddy structures in the LES. They compare well to those obtained by Chu et al. (1996) near the ground, which are nearly-gaussian. A LES for a zero-mean wind convective case has also been made and the PDFs show large departures from gaussianity and compare well to available experimental data (Chu et al, 1996; DW85).

The combined analysis of some cross-sections and their PDFs let us put into correspondence the observed structures and the information provided by the statistical moments. The characteristic functions are computed from the gaussian fit of the PDFs for the SBL and the second order moments are obtained. The gaussianity hypothesis results in the understimation of the intensity of the standard deviation. Moreover, during the eighth hour the horizontal cross-sections are stationary but not homogeneous, and the ergodic theorem is not fulfilled.

The effect of a degradation of the resolution is the lesser statistical representativity of the PDF and coarser structures, with more homogeneous fields and smaller departure from ergodicity.

References

Beare, R.J., MacVean, M.K., Holtslag, A.A.M., Cuxart, J., Esau, I., Golaz, J.-C., Jimenez, M.A., Khairoutdinov, M., Kosovic, B., Lewellen, D., Lund, T.S., Lundquist, J.K., McCabe, A., Moene, A.F., Noh, Y., Raash, S., and Sullivan, P. (2004). An intercomparison of Large-eddy simulations of the stable boundary layer. *Submitted to Boundary-Layer Meteorol.*.

Chu, C.R., Parlange, M.B., Katul, G.G., and Albertson, J.D. (1996). Probability density functions of turbulent velocity and temperature in the atmospheric surface layer. *Water Resources Research* **32**, 1681–1688.

Cuxart, J., Bougeault, P. and Redelsperger, J.-L. (2000). A turbulence scheme allowing for mesoscale and large-eddy simulations. *Q. J. R. Meteorol. Soc.*, **126**, 1–30.

Deardorff, J.W., and Willis, G.E. (1985). Further results from a laboratory model of the convective planetary boundary layer. *Boundary-Layer Meteorol.*, **32**, 205–236.

Lafore, J.P., Stein, J., Asencio, N., Bougeault, P., Ducrocq, V., Duron, J., Fisher, C., Héreil, P., Mascart, P., Masson, V., Pinty, J.P., Redelsperger, J.-L., Richard, E. and Vilà-Guerau de Arellano, J. (1998). The Meso-NH atmospheric simulation system. Part I: Adiabatic formulation and control simulation. *Ann. Geophys.*, **16**, 90-109.

Mahrt, L, and Paumier, J. (1984). Heat transport in the atmospheric boundary layer. *J. Atmos. Sci.*, **41**, 3061–3075.

Nieuwstadt, F.T.M., Mason, P.J., Moeng, C.-H., and Schumann, U. (1993). Large-eddy simulation of the convective boundary layer: A comparison of four computer codes. *Turbulent shear flows 8*, Durst et al., Eds. Springer–Verlag, 343–367.

Tennekes, H. and Lumley, J.L. (1982). A First Course in Turbulence. *The Massachusetts Institute of Technology*, 300pp.

Wilks, D.S. (1995). Statistical methods in the atmospheric sciences. *Academic Press*, 467pp.